JTTEE5 24:611–621
DOI: 10.1007/s11666-015-0218-2
1059-9630/$19.00 © ASM International

Healing of the Interface Between Splashed Particles and Underlying Bulk Coating and Its Influence on Isothermal Oxidation Behavior of LPPS MCrAlY Bond Coat

Bang-Yan Zhang, Jing Shi, Guan-Jun Yang, Cheng-Xin Li, and Chang-Jiu Li

(Submitted June 6, 2014; in revised form December 22, 2014)

The thermally grown oxide formed on the bond coat surface plays an important role in determining the lifetime of thermal barrier coatings (TBCs). The splashed particles on the thermally sprayed MCrAlY bond coat surface are weakly bonded to the underlying bulk coating, leading to the formation of mixed oxides and contributing to the TBC failure. In this study, the healing behavior of the weakly bonded interface between splashed particles and underlying MCrAlY bulk coating deposited by low pressure plasma spraying was examined, and the influence of interface healing on the isothermal oxidation behavior of the bond coat was discussed. Results show that the granular particles resulting from splashing of molten droplets were exposed on smooth splats which make up the surface of bulk coating. After the pre-diffusion treatment in vacuum, the small granular splashed particles are immersed into the bulk coating resulting from the element diffusion on the interface between splashed particles and underlying bulk coating. After the vacuum heat treatment, the formation of mixed oxides was effectively restrained due to the healing of the splashed particle/underlying bulk coating interface.

Keywords bond coat, interface healing, isothermal oxidation, splashed particles, thermal barrier coatings

1. Introduction

Thermal barrier coatings (TBCs) have been widely applied to hot section parts in gas turbines for both aircraft engines and industrial electric power generation (Ref 1-4). TBCs are generally composed of a thermal insulating yttria-stabilized zirconia (YSZ) top coating and a MCrAlY bond coat on a Ni-based superalloy substrate. A thermally grown oxide (TGO), which grows at the interface between the bond coat and the YSZ coating, is actually an additional part of TBCs (Ref 5-7). It is reported that the TGO plays an extremely important role in determining the lifetime of TBCs (Ref 1, 8).

The preparation approach of MCrAlY bond coat and its microstructure is closely related with the durability of the thermal insulating top coating. For atmospheric plasma-sprayed (APS) YSZ top coating, a rough bond coat surface is required to create a better interlocking adhesion. However, such interface morphology produces the out-of-plane stresses responsible for in-service failure (Ref 9), since the out-of-plane stress due to the undulating bond coat surface induces the cracking between the TGO and the bond coat at the undulation crest (Ref 10, 11) and promotes the failure of TBCs (Ref 12).

Theoretically, a stable and slowly grown α-Al_2O_3 TGO is optimal. However, the uniformity along the interface and the constituents of TGO are significantly influenced by the surface morphology of the bond coat before YSZ deposition (Ref 9, 13). Besides α-Al_2O_3 scale, Cr_2O_3, NiO, and $(Ni,Co)(Cr,Al)_2O_4$ may be present in TGO. A different composition of TGO is associated with different failure mechanisms of TBCs (Ref 14). The formation of Cr_2O_3, being a protective scale against corrosion, needs a relatively high-critical oxygen partial pressure when compared with the formation of α-Al_2O_3 (Ref 15). However, it changes to CrO_3 at a temperature higher than 1000 °C and an oxygen partial pressure range of 0.1-10^{-4} MPa (Ref 16). NiO tends to grow in an atmosphere of a high oxygen partial pressure (Ref 17). Spinels, stoichiometrically expressed as $(Ni,Co)(Cr,Al)_2O_4$ (Ref 18), are porous and brittle (Ref 19). Therefore, many investigations (Ref 12-14) were conducted to aim at controlling the TGO structure.

Cold spraying is an emerging coating process, involving high-velocity impact of solid powder particles (Ref 20-23). Coating is formed through plastic deformation upon impact of spray particles, temperatures of which are much lower than the melting point of spray material. The

This article is an invited paper selected from presentations at the 2014 International Thermal Spray Conference, held May 21-23, 2014, in Barcelona, Spain, and has been expanded from the original presentation.

Bang-Yan Zhang, Jing Shi, Guan-Jun Yang, Cheng-Xin Li, and **Chang-Jiu Li**, State Key Laboratory for Mechanical Behavior of Materials, School of Materials Science and Engineering, Xi'an Jiaotong University, Xi'an 710049, Shaanxi, People's Republic of China. Contact e-mails: ygj@mail.xjtu.edu.cn and licj@mail.xjtu.edu.cn.

undulated surface morphology of spray particles may be retained to the coating surface layer (Ref 24-26). Splashing resulting from spray droplet impact can be well restrained. By comparatively examining the thermal cycling performance of TBCs with cold sprayed bond coat or low-pressure plasma sprayed (LPPS) bond coat, it was proved that the splashed particles and the resulting mixed oxides are the main reason for the relatively shorter lifetime of TBCs with LPPS bond coat compared to cold-sprayed bond coat (Ref 27). Therefore, it is of importance to restrain or completely eliminate the mixed oxides in TGO for the LPPS bond coat for prolonging the lifetime of TBCs.

In this study, the LPPS bond coat was subjected to different pre-treatments before the isothermal oxidation in air. The healing behavior of the interface between splashed particles and underlying bulk coating and its influence on oxidation behavior were examined to aim at developing durable TBCs with LPPS bond coat.

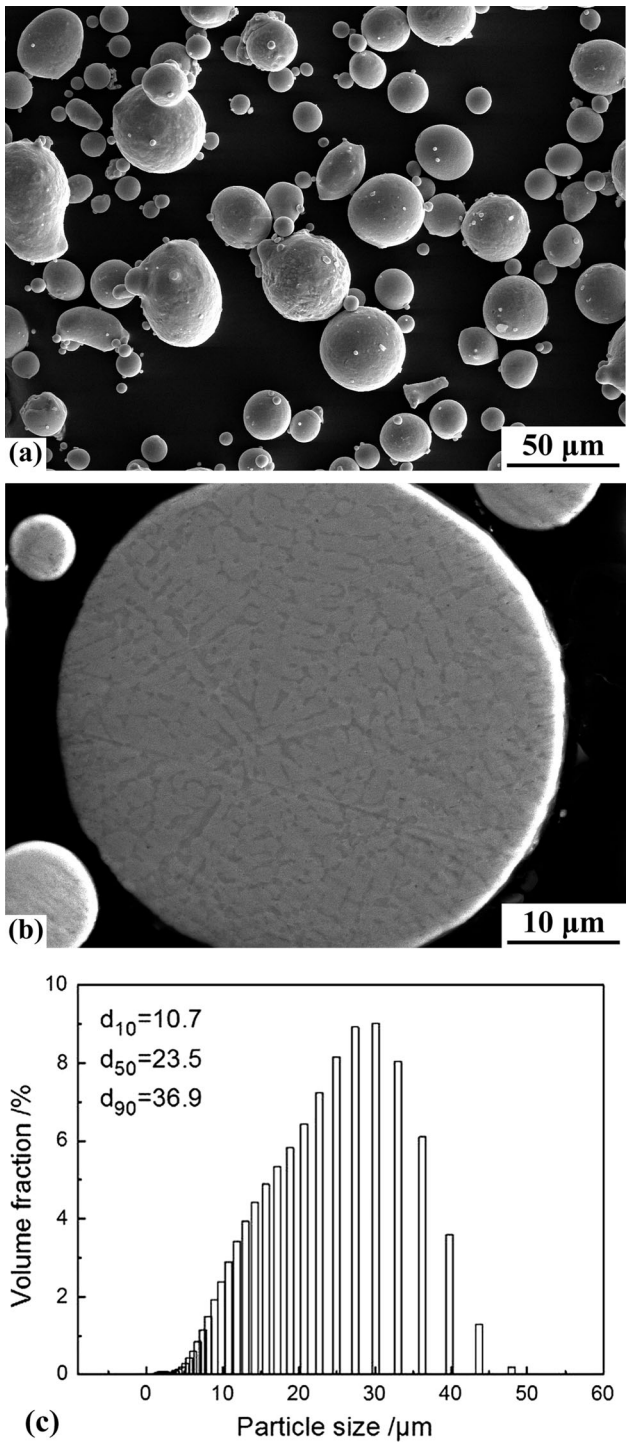

Fig. 1 Surface morphology (a), cross-sectional structure (b) and particle size distribution (c) of the CoNiCrAlY feedstock powder

2. Experimental Procedure

2.1 Materials

The bond coats of ~150 μm in thickness were deposited by LPPS, using CoNiCrAlY powder particles in a spherical shape (Amdry 9951, Sulzer-Metco, USA). The surface morphology and cross-sectional structure of the powder are shown in Fig. 1(a) and (b). Figure 1(c) shows the particle size distribution ($d_{10} = 10.7$ μm, $d_{90} = 36.9$ μm) with a mean particle size of ~23.5 μm. The nominal element content (wt.%) of the feedstock powder is shown in Table 1. Nickel-based superalloy Inconel 738 (ϕ 25.4 mm × 3 mm) was used as a substrate.

2.2 Coating Deposition and Treatment

The LPPS spray conditions are shown in Table 2. In the LPPS process, high-purity argon (Ar ≥ 99.999%, O_2 ≤ 1.5 ppm) was chosen as the main gas for spraying and the powder feeding gas, and high-purity hydrogen was chosen as the auxiliary gas for spraying. The pressure in the chamber was reduced to a low pressure below 50 Pa before spraying, and then the chamber was filled with

Table 1 Elements' nominal content (wt.%) of the feedstock powder

Elements	Co	Ni	Cr	Al	Y
Nominal content, wt.%	Bal.	32	21	8	0.5

Table 2 LPPS conditions

Parameters	Value
Arc power, kW	45
Arc current, A	620
Arc voltage, V	72
Plasma gas (Ar) flow, L/min	40
Plasma gas (H_2) flow, L/min	8
Powder feeding gas (Ar) flow, L/min	2
Chamber pressure, kPa	15
Spray distance, mm	160
Torch traverse speed, mm/s	100

Table 3 Pre-treatment conditions

Pre-treatment	Environment	Temperature and duration
Pre-oxidation	Ar (Ar ≥ 99.99%, $P(O_2)$ < 3 Pa)	4 h at 1000 °C + 4 h at 1080 °C
Pre-diffusion	High vacuum ($P(O_2)$ < 0.002 Pa)	1150 °C for 3 h

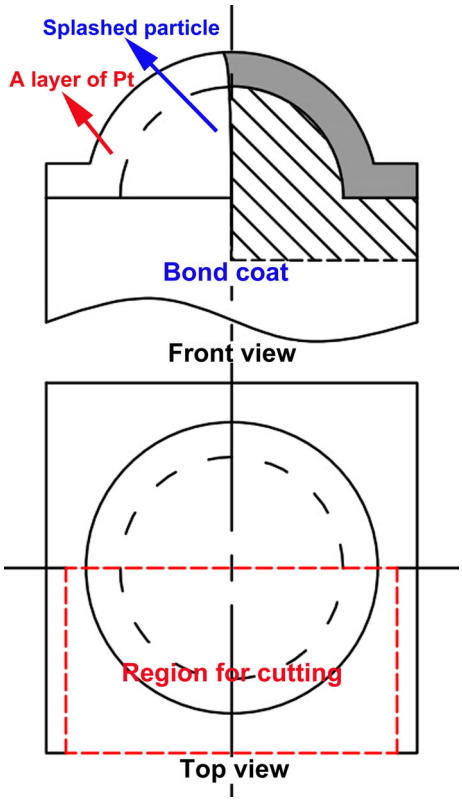

Fig. 2 Schematic diagram of cutting the splashed particle by FIB

argon (Ar ≥ 99.99%, O_2 ≤ 10 ppm) to a pressure of 70 kPa for igniting the plasma torch. After ignition, the LPPS bond coat was deposited in a vacuum chamber at a chamber pressure of 15 kPa charged with argon (Ar ≥ 99.99%, O_2 ≤ 10 ppm).

The as-sprayed bond coats were subjected to pre-treatment by two different approaches prior to isothermal oxidation in air. One approach, pre-oxidation, included only a pre-oxidation conducted in Ar. The other approach, pre-diffusion-oxidation, included a pre-diffusion in vacuum followed by the pre-oxidation treatment mentioned above. The detailed parameters of pre-diffusion and pre-oxidation treatments are shown in Table 3. The pre-diffusion can make small particles on the bond coating surface have a good bonding with the underlying bulk coating, which will be further shown in the results part. The pre-oxidation treatment was used to form a sufficiently thick and continuous oxide scale on the surface of the bond coats to suppress inward diffusion of oxygen and outward diffusion of cation during the subsequent high temperature isothermal oxidation in air. After pre-

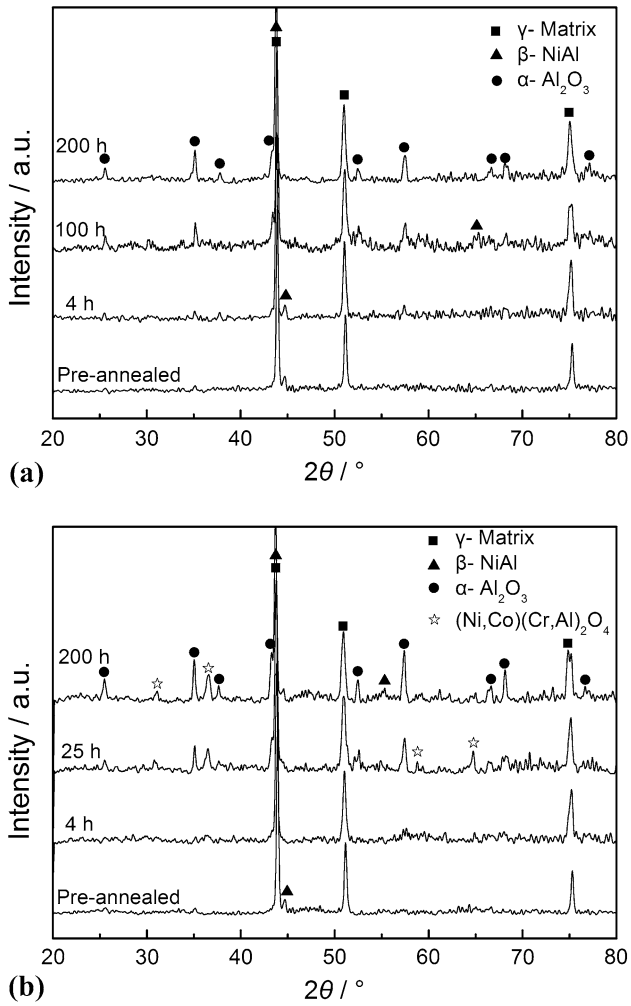

Fig. 3 XRD patterns of coatings after isothermal oxidation in air. (a) Pre-diffusion-oxidation coating, (b) pre-oxidation coating

treatments, the bond coats were subjected to isothermal oxidation for different durations (4, 25, 100, and 200 h) at 1000 °C in air.

2.3 Characterization

For better observation of the bond between the splashed particles on the surface of the pre-diffused coatings and the underlying coating surface, the splashed particles were cut at the maximum diameter in the vertical direction of the particles surface by high-speed, focused Ga ions with the focused ion beam (FIB, Helios NanoLab 600, FEI, USA) tool. A layer of Pt was deposited on the splashed particles surface before cutting to protect the top

of the splashed particles for a vertical section and to mark the position of the interested particles. The schematic of cutting the splashed particle by FIB is shown in Fig. 2. The region surrounded by the red rectangular wireframe (dashed lines) in Fig. 2 is for cutting by FIB.

To prove the diffusion connection between the splashed particles and the underlying bond coat surface, the spherical Ni particles ($d_{50} \geq 1$ μm, LNi-II, LLEEU, China) with a comparable size to the splashed particles were diffused into the Ni substrate at a low partial pressure of oxygen ($P(O_2) < 1$ Pa) under different temperatures (1000, 1050, and 1100 °C) for 2 h. The Ni particles and Ni substrate have the same elements' nominal content (Ni ≥ 99.9%). The reason to choose Ni rather than MCrAlY herein is that the oxide scale covered on the Ni particle surface can be completely avoided by using a reduction atmosphere.

The surface roughness of the as-sprayed bond coat and the bond coats with different pre-treatments was measured by color 3D laser scanning microscope (VK-9710, KEYENCE, Japan). The crystalline structure of TGO was characterized by x-ray diffraction analysis (XRD, D8advance 3.0, Bruker, Germany). The surface morphology and cross-sectional microstructure of coatings and TGO

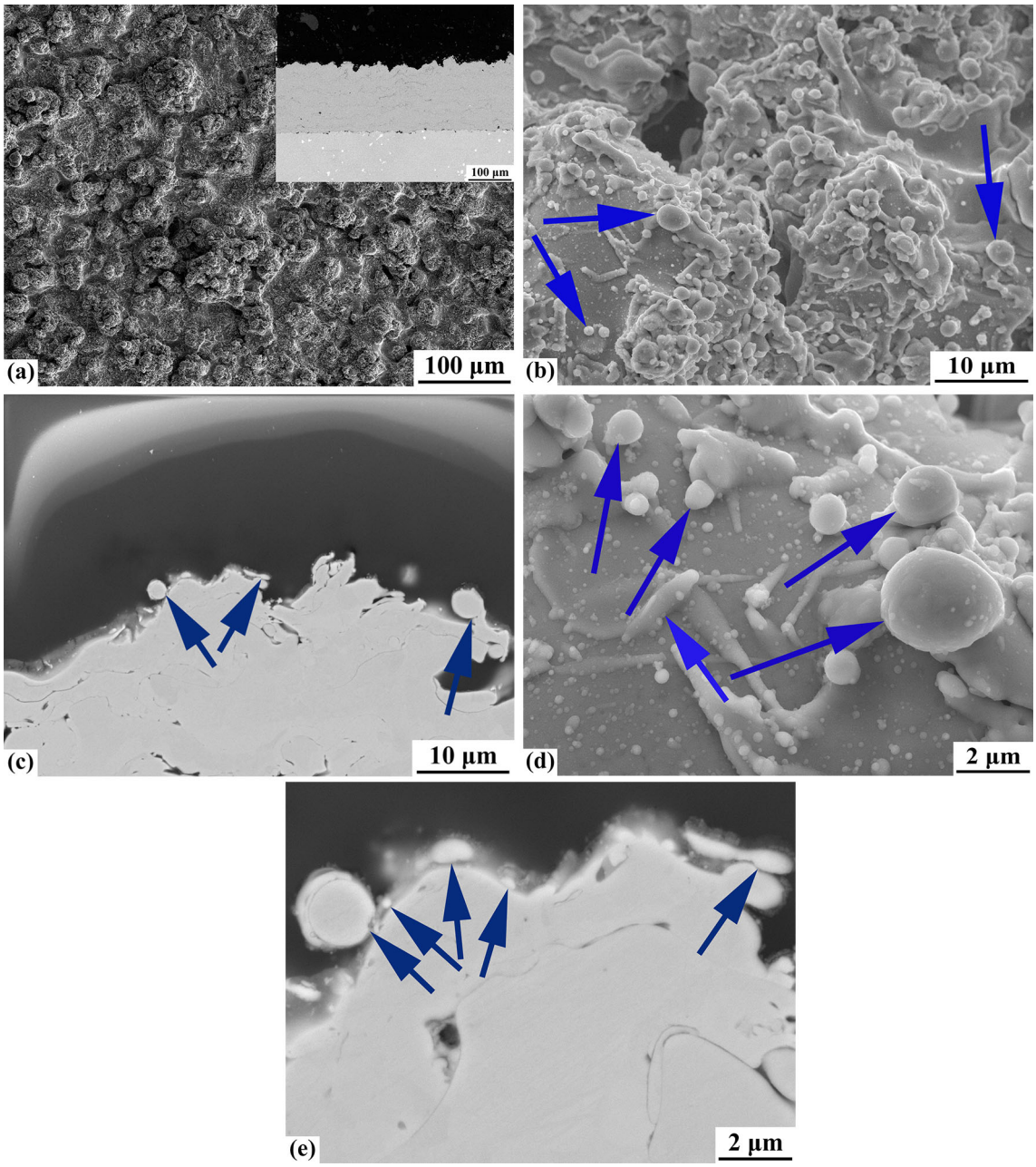

Fig. 4 Low-magnification image (a) and high-magnification images (b-e) of the microstructure of the as-sprayed bond coat. (b, d) Surface morphology, (c, e) cross-sectional microstructure

were examined by field emission scanning electron microscope (SEM, MIRA 3 LMH, TESCAN, Czech Republic). Ni-electroless plating was used to deposit a layer of Ni on the bond coat surface to protect the TGO scale from spalling off during the cutting and polishing of samples.

3. Results and Discussion

3.1 XRD Patterns of the Coatings After Isothermal Oxidation

Figure 3 shows the XRD patterns of the coatings after isothermal oxidation in air. For the pre-diffusion-oxidation coating (Fig. 3a), only Al_2O_3 TGO can be found up to oxidation duration of 200 h. However, for the pre-oxidation coating (Fig. 3b), mixed oxides ($(Ni,Co)(Cr,Al)_2O_4$) formed after 25 h. To further understand the reason of the above phenomenon, the microstructure of the bond coats was observed.

3.2 Microstructure of Splashed Particles on LPPS Coating Surface

Figure 4 shows the topographical morphology and cross-sectional microstructure of the LPPS as-sprayed bond coat. Figure 4(a) presents a rough surface morphology ($Ra = 13.3 \pm 1.1$ μm), which is a typical characteristic of thermally sprayed coatings, resulting from the random stacking of splats. This rough surface morphology would be useful to improve the adhesion of thermal insulating top coating to bond coat surface. The surface roughness results from two kinds of particles on the coating surface according to Fig. 4. On the coating surface, there are many particular convexes (Fig. 4a), with a size (dozens of micrometers) comparable to the feedstock powder (Fig. 1), resulting from the semi-molten particles (Ref 27-29). In addition, high-magnification image (Fig. 4b and d) clearly reveals some small granular particles and longish needles in a size range from submicrometers to several micrometers, being much smaller than the feedstock powder. These particles were produced by the splashing of liquid droplets impacting on deposited surface with a rough topographical morphology (Ref 27). The two kinds of splashed particles have the same influence on the properties of TBCs. The granular splashed particles were chosen as the study object in the following discussion because they were more representative and conveniently statistical. It can be found from the cross-sectional microstructure (Fig. 4c and e) that the splashed particles are weakly bonded to the underlying coating surface.

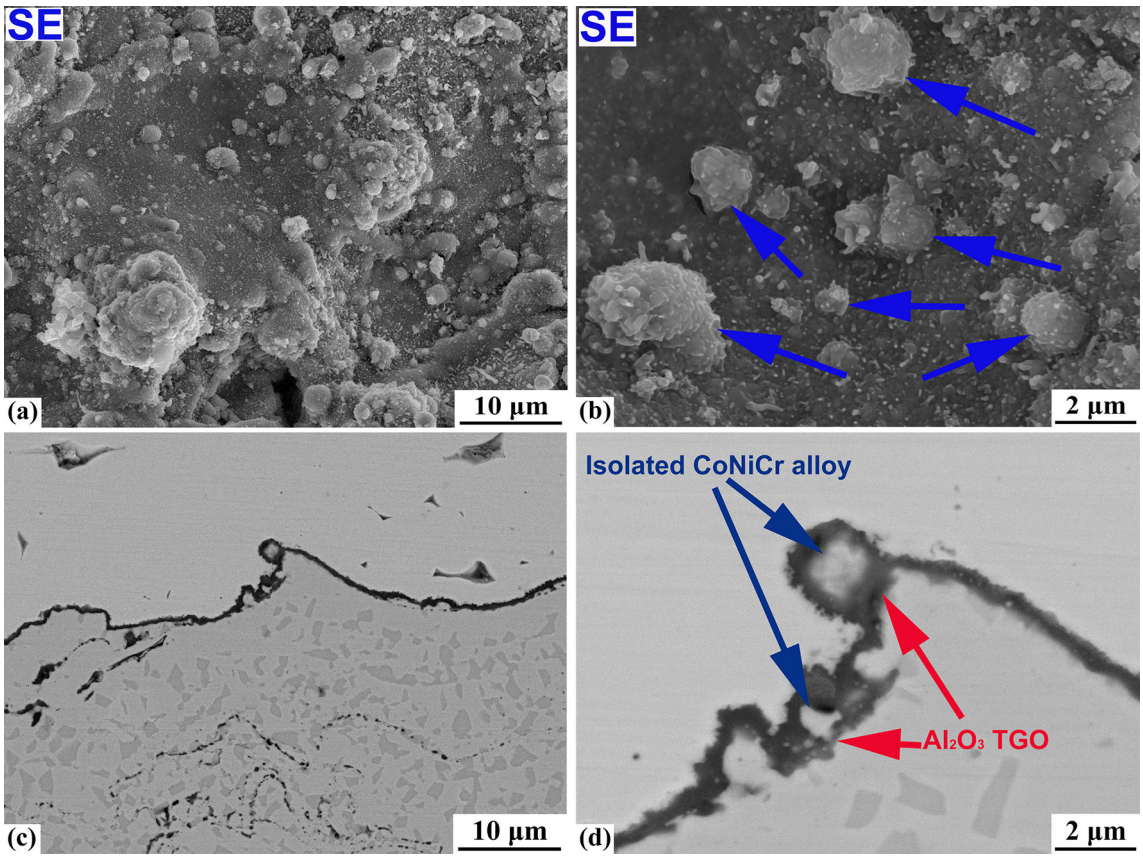

Fig. 5 Surface morphology (a, b) and cross-sectional microstructure (c, d) of pre-oxidation bond coats

3.3 Particle/Bulk Interface Healing Behavior During Pre-treatments

3.3.1 The Microstructure of the Pre-oxidation Bond Coats. Figure 5 shows the microstructure of the bond coat after pre-oxidation. Many granular particles can be found from the surface morphologies of the coating (Fig. 5a and b). The size of the granular particles (The average size of the splashed particles is 1.3 ± 0.8 μm.) in Fig. 5a and b seems comparable to the splashed metallic particles (The average size of the splashed particles is 1.2 ± 0.5 μm.) in Fig. 4(b)-(e). It can be found from Fig. 5(c) and (d) that a continuous Al_2O_3 TGO, with a mean thickness of ~0.5 μm, is formed on the coating surface including both the relatively smooth surface ($Ra = 12.9 \pm 2.8$ μm) and the splashed particles. Furthermore, it is interestingly found that the surface particles on coating surface present a core-shell structure with a Al_2O_3 scale covering the granular metallic core, which results from the poor bonding between the surface particles and the underlying coating surface. The core-shell structure can result in pre-generation of the mixed oxides because of insufficient diffusion effect of Al element (Ref 27, 30) between the granular metallic core and the metallic bond coat in the process of oxidation, which can bring forward the failure of the TBCs.

3.3.2 The Microstructure of the Pre-diffused Coatings. Compared to the pre-oxidation samples, the pre-diffused coatings present much different microstructure as shown in Fig. 6. The coating after pre-diffusion presents a relatively smooth surface morphology ($Ra = 12.5 \pm 1.8$ μm) with a TGO layer. Figure 6(b) shows a splashed particle in a diameter of ~4 μm on the pre-diffused coatings, and its cross-sectional microstructure (Fig. 6c) was obtained by FIB technology. It can be found from Fig. 6(c) that the original weakly bonded granular splashed particles have been well bonded to the underlying coating surface through elements diffusion at high temperature, and the incontinuous Al_2O_3 (black arrows in Fig. 6c) can be distinguished at the interface between the splashed particles and the underlying coating surface. Figure 6 reveals that the very small submicron splashed particles have diffused into the underlying bulk coating, and the micron particles have a larger size than the particles on the surface of as-sprayed bond coats because of their spreading in the pre-diffusion process. To further prove the diffusion connection between splashed particles and underlying bond coat surface, Ni particle/Ni substrate system without oxide inter-layer, used to mimic the splashed particles on bond coat surface, was subjected to high-temperature exposure at different temperatures, as shown in Fig. 7. Upon the thermal exposure at 1000-1100 °C for a duration of 2 h, all the Ni particles with a size of several micrometers diffused into the Ni lath to form a bump surface morphology. Thus, the disappearance of submicron-sized splashed particles after a pre-diffusion at 1150 °C for 3 h can be attributed to the full diffusion into the underlying coating surface. Therefore, the healing of the interface between splashed particles and underlying coating surface contributed to the formation of a relatively smooth coating surface and effective bonding condition between large sized splashed particles and underlying coating surface.

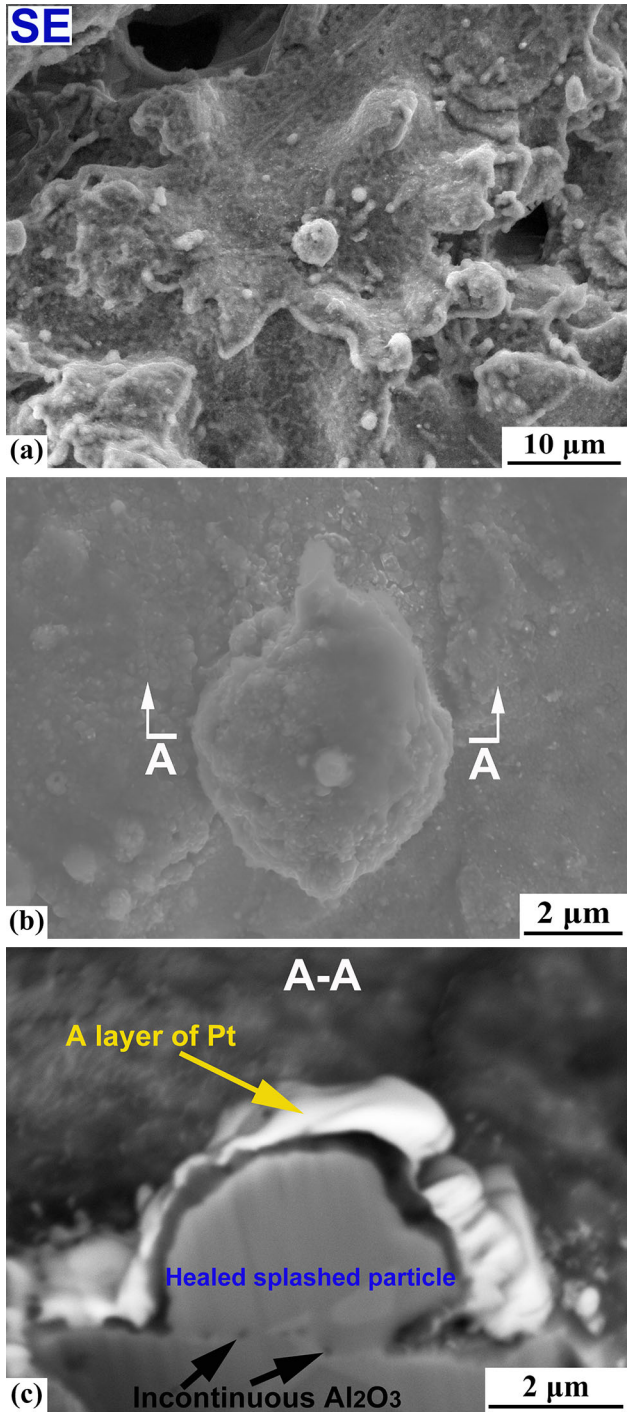

Fig. 6 Microstructure of pre-diffused bond coats. A splashed particle (b) on the pre-diffused coatings surface and its cross-sectional microstructure (c) obtained by FIB

3.4 Breaking of Oxide Scale Between Splashed Particles and Underlying Bond Coat

It is worth to note that there is an oxide scale between splashed particles and the underlying bond coat surface. The diffusion of splashed particles into the underlying bond coat surface is capable to occur only if the oxide scale has been

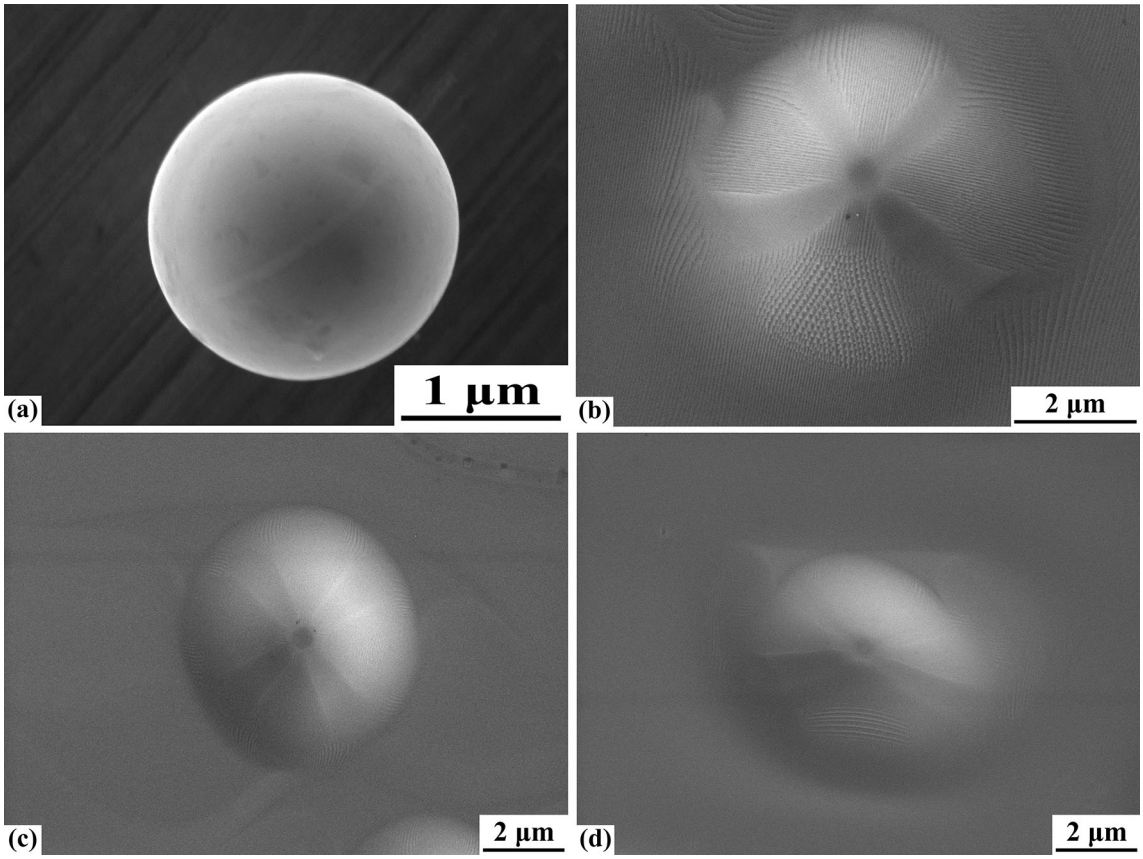

Fig. 7 Ni particles diffusion into Ni lath after heat treatment. (a) Original state, (b) 2 h at 1000 °C, (c) 2 h at 1050 °C, (d) 2 h at 1100 °C

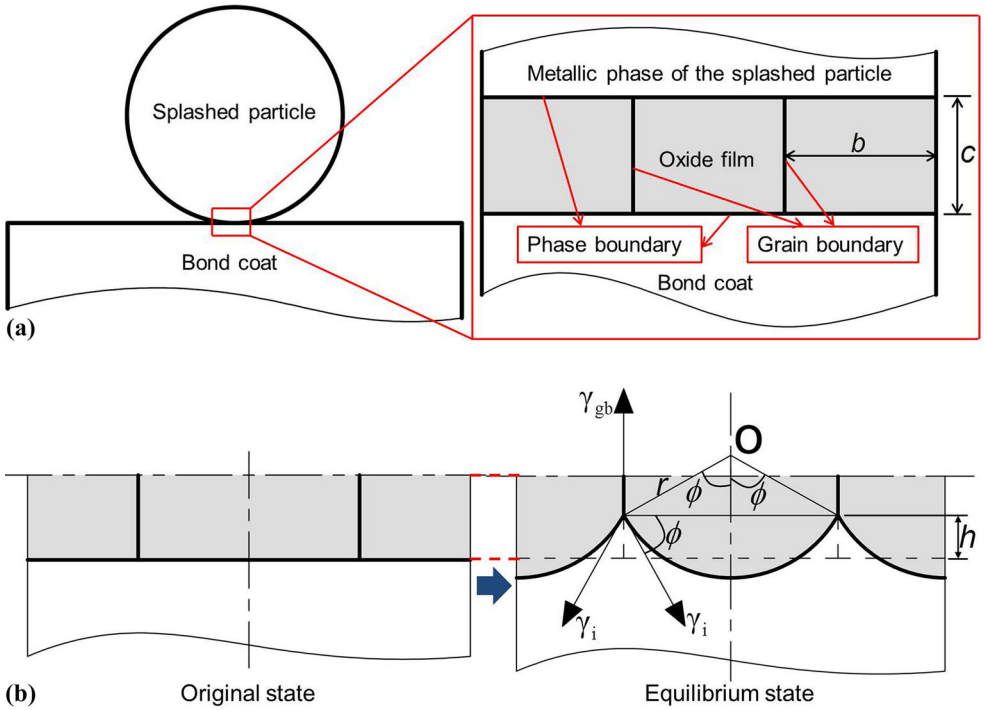

Fig. 8 The profile (a) and the thermal grooving at the phase interface (b) of the object of study

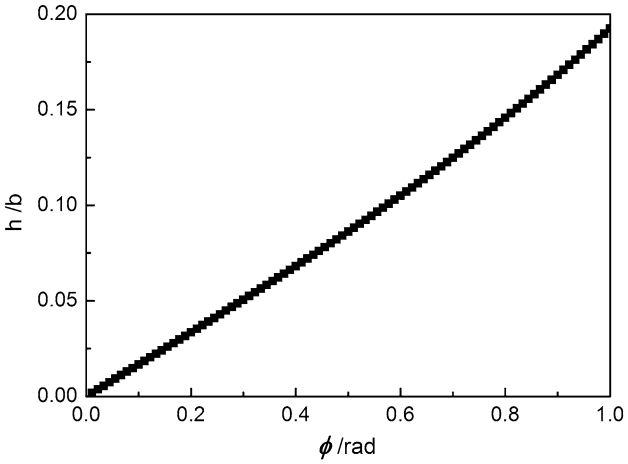

Fig. 9 The relationship between ϕ and h

broken providing an effective route for the element diffusion. It is obvious that the breaking of oxide scale is more difficult with the increase of oxide scale thickness. In order to better understand the influence of the oxide scale thickness on the oxide scale breaking, a simple model shown in Fig. 8 was proposed to obtain the oxide scale thickness limit for breaking. Thermal grooving of grain boundaries of oxide scale is the main reason for the oxide scale breaking, and thermodynamics is used for the computational process. It is assumed that the thickness of the oxide scale and the oxide grain are infinite homogeneous sheets. And the oxide grains' size perpendicular to the direction of the paper is infinite, which can simplify calculation. It is also assumed that the oxide scale is of two-dimensional structure, and the cross-sectional structure is shown in Fig. 8(a). Due to the symmetry of the oxide scale to the two-side bond coat material, Fig. 8(b) only shows the half model of the oxide scale. The theoretical basis of this process is the following thermodynamic equations:

$$2\gamma_i \sin\phi = \gamma_{gb}, \qquad \text{(Eq 1)}$$

where γ_i is the energy density of the interface between oxide scale and bond coat material, γ_{gb} is the grain boundary energy density of oxide scale, and ϕ is grain boundary grooving angle. This equation describes the energy equilibrium at the cross of two phase boundaries and one grain boundary. Generally, γ_i is between γ_{gb} and γ_s (the surface energy density of the oxide scale), and γ_{gb} is often one-third of γ_s. Consequently, the value of ϕ can be estimated to be in a range from 0.167 to 0.524 rad.

After the grain boundary thermal grooving, a depth (h) of the original flat phase boundary can be formed. Based on the mass conversation rule, h can be expressed by the following equation:

$$h = \frac{b}{4\sin^2\phi}(\phi - \sin\phi\cos\phi), \qquad \text{(Eq 2)}$$

where b is the grain size of oxide scale. It can be found from Fig. 9 that h increases monotonously with ϕ. Therefore, the maximum (h_{max}) and minimum (h_{min}) of h can be reached for the maximum and minimum of ϕ, respectively,

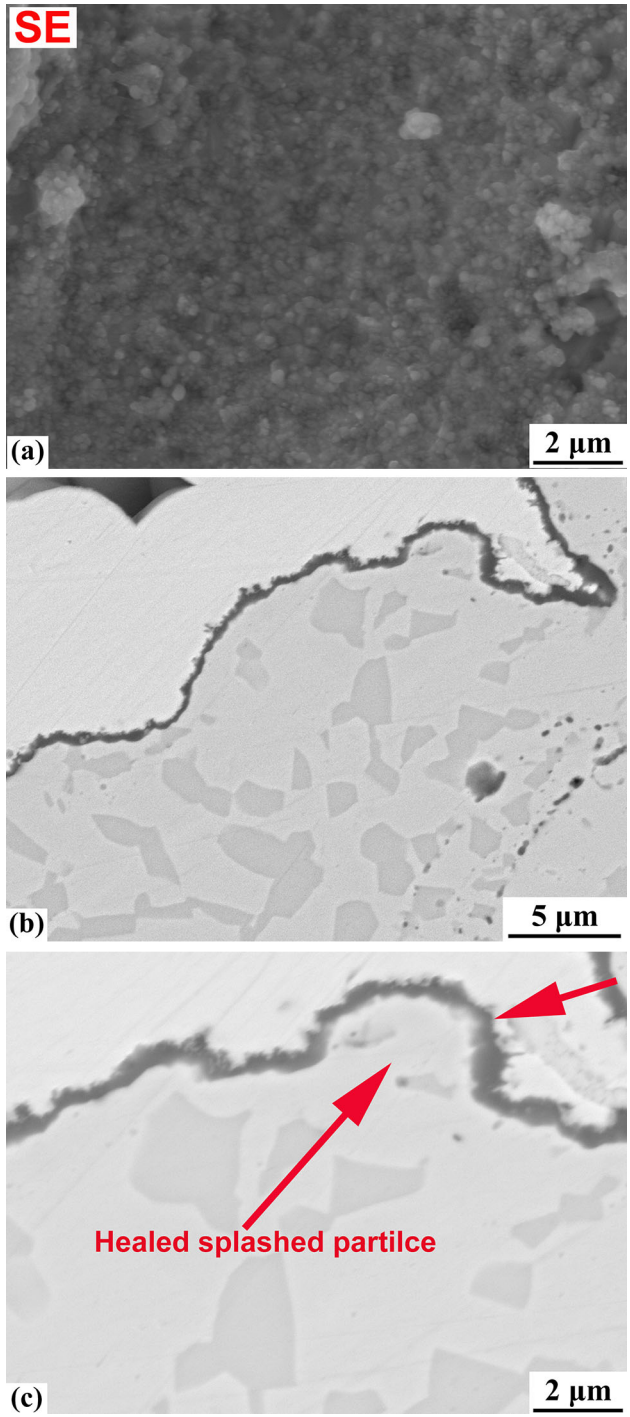

Fig. 10 Surface morphology (a) and cross-sectional microstructure (b, c) of pre-diffusion-oxidation samples

$$h_{max} \approx 0.091b \text{ when } \gamma_i = \gamma_{gb} \qquad \text{(Eq 3)}$$

$$h_{min} \approx 0.023b \text{ when } \gamma_i = \gamma_s. \qquad \text{(Eq 4)}$$

The Eq 3 and 4 can reveal the relationship between the oxide grain size in in-plane direction and the depth of the

thermal groovings of oxide scale grain boundary. They indicate that the thickness of the oxide scale plays an important role in the scale breaking. It can be found that interface healing between the splashed particles and underlying bond coat through element diffusion at high temperature can happen when the thickness of the oxide scale is sufficiently small.

Figure 10 shows the microstructure of the pre-diffusion-oxidation samples. From Fig. 6(a) and 10(a), it can be seen that the pre-oxidation seems not to change the surface morphology of the coating. The surface roughness ($Ra = 12.2 \pm 0.4$ μm) of the pre-diffusion-oxidation bond coat (Fig. 10a) is comparable to the pre-diffused bond coat ($Ra = 12.5 \pm 1.8$ μm, Fig. 6a). A continuous Al_2O_3 scale can be found on the coating surface. The TGO thickness of ~0.5 μm is comparable with the pre-oxidation samples. Due to the good bonding condition between the large splashed particles and underlying bond coat, the core-shell structure shown in the pre-oxidation samples is seldom found in the pre-diffusion-oxidation samples.

3.5 Effect of Interface Healing on Isothermal Oxidation Behavior

From the above discussion, it can be seen that it is the healing of the interface between splashed particles and underlying bulk coating that keeps the Al_2O_3 TGO longer on the surface of the pre-diffusion-oxidation bond coats than the pre-oxidation bond coats. To further understand the formation of mixed oxides for pre-oxidized coating, the cross-sectional TGO structure of bond coat with different pre-treatments and isothermal oxidation is observed and shown in Fig. 11. It can be seen that the mixed oxides were formed on the TGO surface region. Similar mixed oxides have been reported in the literature (Ref 30). The generation of the mixed oxides on TGO surface region is ascribed to the exhausting of Al element in the surface particles because the Al diffusion from the inner bond coat to the surface particles was obstructed by the oxide formed at the interface between surface particles and the underlying bulk bond coat (Ref 30). Figure 11(b) and (d) show that only a few isolated mixed oxides can be found on the pre-diffusion-oxidation coating surface after isothermal oxidation of 100 h, but the TGO on the pre-oxidation bond coats after isothermal oxidation of 100 h presents a bi-layered structure, i.e., outside mixed oxides and inside Al_2O_3. The results show that the pre-diffusion treatment can suppress the growth of mixed oxides, which is potentially good for the TBCs lifetime.

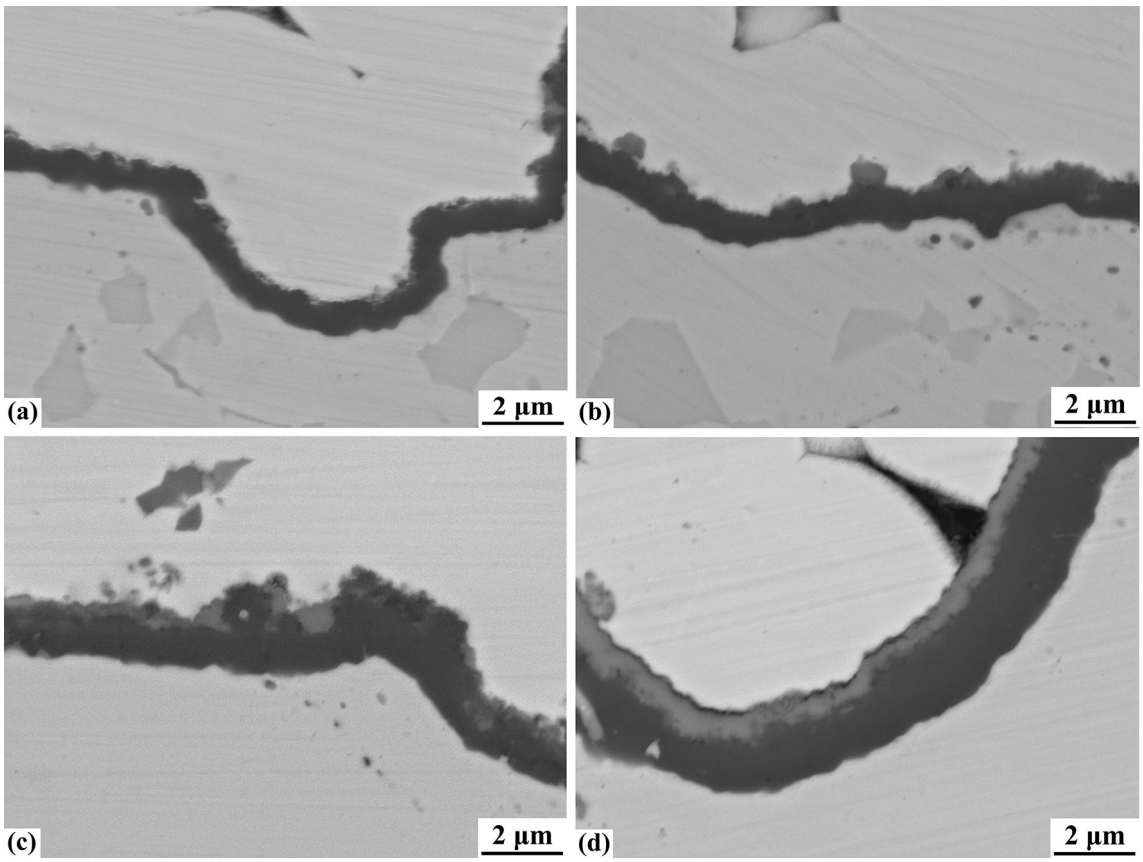

Fig. 11 The TGO structure of bond coats with different pre-treatments and isothermal oxidation. (a) With pre-diffusion-oxidation and 25 h isothermal oxidation at 1000 °C, (b) with pre-diffusion-oxidation and 100 h isothermal oxidation at 1000 °C, (c) with pre-oxidation and 25 h isothermal oxidation at 1000 °C, (d) with pre-oxidation and 100 h isothermal oxidation at 1000 °C

4. Summary

CoNiCrAlY bond coat deposited by LPPS shows a rough surface morphology resulting from both the semi-melted powder particles and the splashed particles (in a size range from sub-micrometre to several micrometres) weakly bonded to the underlying coating surface. The surface morphology and microstructure of the bond coats with different pre-treatments were examined. Results show that the pre-oxidation ($P(O_2) < 3$ Pa in Ar) leads to a continuous Al_2O_3 TGO on bond coat surface, and the splashed particles presents a core-shell structure with CoNiCr metallic phase covered by Al_2O_3 scale. Meanwhile, the pre-oxidation resulted in the formation of mixed oxides on the outer surface of TGO after the isothermal oxidation for 25 h at 1000 °C. However, isolated CoNiCr alloy within TGO could be hardly found after interface healing between splashed particles and underlying coating occurred during the pre-diffusion. A calculation model of the oxide scale breaking at high temperature is provided to better understand the influence of the thin oxide scale thickness on the oxide scale breaking. By the calculation, it can be seen that the thickness of the oxide scale plays an important role in the scale breaking according to the thermodynamics. As a result, no obvious mixed oxides are found during the isothermal oxidation for 100 h at 1000 °C in air. In brief, interface healing between the splashed particles and underlying coating can avoid the generation of the mixed oxides on TGO surface and thereby potentially benefit the lifetime of TBCs.

Acknowledgments

The present project is supported by National Basic Research Program (Grant No. 2013CB035701), National Program for Support of Top-notch Young Professionals, and the Fundamental Research Funds for the Central Universities.

References

1. A.G. Evans, D.R. Mumm, J.W. Hutchinson, G.H. Meier, and F.S. Pettit, Mechanisms Controlling the Durability of Thermal Barrier Coatings, *Prog. Mater. Sci.*, 2001, **46**(5), p 505-553
2. W.J. Brindley, Thermal Barrier Coatings, *J. Therm. Spray Technol.*, 1996, **5**(4), p 379-380
3. T. Strangman, D. Raybould, A. Jameel, and W. Baker, Damage Mechanisms, Life Prediction, and Development of EB-PVD Thermal Barrier Coatings for Turbine Airfoils, *Surf. Coat. Technol.*, 2007, **202**(4-7), p 658-664
4. Q. Zhang, C.-J. Li, Y. Li, S.-L. Zhang, X.-R. Wang, G.-J. Yang, and C.-X. Li, Thermal Failure of Nanostructured Thermal Barrier Coatings with Cold-Sprayed Nanostructured NiCrAlY Bond Coat, *J. Therm. Spray Technol.*, 2008, **17**(5-6), p 838-845
5. S. Ahmaniemia, P. Vuoristoa, T. Mantyla, C. Gualco, A. Bonadei, and R. Di Maggio, Thermal Cycling Resistance of Modified Thick Thermal Barrier Coatings, *Surf. Coat. Technol.*, 2005, **190**(2-3), p 378-387
6. T. Vogt, B.A. Hunter, and J. Thornton, Structural Evolution of Thermal-Sprayed Yttria-Stabilized ZrO_2 Thermal Barrier Coatings with Annealing—A Neutron Diffraction Study, *J. Am. Ceram. Soc.*, 2001, **84**(3), p 678-680
7. S. Bose and J.D. Marcin, Thermal Barrier Coating Experience in Gas Turbine Engines at Pratt & Whitney, *J. Therm. Spray Technol.*, 1997, **6**(1), p 99-104
8. N.P. Padture, M. Gell, and E.H. Jordan, Materials Science—Thermal Barrier Coatings for Gas-Turbine Engine Applications, *Science*, 2002, **296**(5566), p 280-284
9. A. Hesnawi, H.-F. Li, Z.-H. Zhou, S.-K. Gong, and H.-B. Xu, Effect of Surface Condition During Pre-oxidation Treatment on Isothermal Oxidation Behavior of MCrAlY Bond Coat Prepared by EB-PVD, *Surf. Coat. Technol.*, 2007, **201**(15), p 6793-6796
10. K.W. Schlichting, N.P. Padture, E.H. Jordan, and M. Gell, Failure Modes in Plasma-Sprayed Thermal Barrier Coatings, *Mater. Sci. Eng. A*, 2003, **342**(1-2), p 120-130
11. F.-H. Yuan, Z.-X. Chen, Z.-W. Huang, Z.-G. Wang, and S.-J. Zhu, Oxidation Behavior of Thermal Barrier Coatings with HVOF and Detonation-Sprayed NiCrAlY Bondcoats, *Corros. Sci.*, 2008, **50**(6), p 1608-1617
12. F. Tang and J.M. Schoenung, Local Accumulation of Thermally Grown Oxide in Plasma-Sprayed Thermal Barrier Coatings with Rough Top-Coat/Bond-Coat Interfaces, *Scripta Mater.*, 2005, **52**(9), p 905-909
13. A. Gil, V. Shemet, R. Vassen, M. Subanovic, J. Toscano, D. Naumenko, L. Singheiser, and W.J. Quadakkers, Effect of Surface Condition on the Oxidation Behaviour of MCrAlY Coatings, *Surf. Coat. Technol.*, 2006, **201**(7), p 3824-3828
14. K. Ogawa, K. Ito, T. Shoji, D.W. Seo, H. Tezuka, and H. Kato, Effects of Ce and Si Additions to CoNiCrAlY Bond Coat Materials on Oxidation Behavior and Crack Propagation of Thermal Barrier Coatings, *J. Therm. Spray Technol.*, 2006, **15**(4), p 640-651
15. W.-R. Chen, R. Archer, X. Huang, and B.R. Marple, TGO Growth and Crack Propagation in a Thermal Barrier Coating, *J. Therm. Spray Technol.*, 2008, **17**(5-6), p 858-864
16. R.-F. Zhou, Y.-F. Han, and S.-S. Li, *High Temperature Structure Materials*, National Defense Industry Press, Beijing, 2006 (in Chinese)
17. R.D. Maier, C.M. Scheuermann, and C.W. Andrews, Degradation of a 2-Layer Thermal Barrier Coating Under Thermal Cycling, *Am. Ceram. Soc. Bull.*, 1981, **60**(5), p 555-560
18. M. Matsumoto, K. Hayakawa, S. Kitaoka, H. Matsubara, H. Takayama, Y. Kagiya, and Y. Sugita, The Effect of Preoxidation Atmosphere on Oxidation Behavior and Thermal Cycle Life of Thermal Barrier Coatings, *Mater. Sci. Eng. A*, 2006, **441**(1-2), p 119-125
19. V. Teixeira, M. Andritschky, W. Fischer, H.P. Buchkremer, and D. Stover, Effects of Deposition Temperature and Thermal Cycling on Residual Stress State in Zirconia-Based Thermal Barrier Coatings, *Surf. Coat. Technol.*, 1999, **120**, p 103-111
20. K.H. Kim, M. Watanabe, and S. Kuroda, Thermal Softening Effect on the Deposition Efficiency and Microstructure of Warm Sprayed Metallic Powder, *Scripta Mater.*, 2009, **60**(8), p 710-713
21. W.-Y. Li, X.-P. Guo, C. Verdy, L. Dembinski, H.-L. Liao, and C. Coddet, Improvement of Microstructure and Property of Cold-Sprayed Cu-4 at.%Cr-2 at.%Nb Alloy by Heat Treatment, *Scripta Mater.*, 2006, **55**(4), p 327-330
22. K. Balani, A. Agarwal, S. Seal, and J. Karthikeyan, Transmission Electron Microscopy of Cold Sprayed 1100 Aluminum Coating, *Scripta Mater.*, 2005, **53**(7), p 845-850
23. Y. Li, C.-J. Li, Q. Zhang, G.-J. Yang, and C.-X. Li, Influence of TGO Composition on the Thermal Shock Lifetime of Thermal Barrier Coatings with Cold-Sprayed MCrAlY Bond Coat, *J. Therm. Spray Technol.*, 2010, **19**(1-2), p 168-177
24. W.-Y. Li, H.-L. Liao, C.-J. Li, G. Li, C. Coddet, and X.-F. Wang, On High Velocity Impact of Micro-sized Metallic Particles in Cold Spraying, *Appl. Surf. Sci.*, 2006, **253**(5), p 2852-2862
25. M. Grujicic, C.L. Zhao, W.S. DeRosset, and D. Helfritch, Adiabatic shear Instability Based Mechanism for Particles/Substrate Bonding in the Cold-Gas Dynamic-Spray Process, *Mater. Des.*, 2004, **25**(8), p 681-688
26. W.-Y. Li, C. Zhang, X.-P. Guo, C.-J. Li, H.-L. Liao, and C. Coddet, Study on Impact Fusion at Particle Interfaces and Its Effect on Coating Microstructure in Cold Spraying, *Appl. Surf. Sci.*, 2007, **254**(2), p 517-526

27. Y. Li, C.-J. Li, G.-J. Yang, and L.-K. Xing, Thermal Fatigue Behavior of Thermal Barrier Coatings with the MCrAlY Bond Coats by Cold Spraying and Low-Pressure Plasma Spraying, *Surf. Coat. Technol.*, 2010, **205**(7), p 2225-2233
28. P. Fauchais, M. Vardelle, A. Vardelle, and L. Bianchi, Plasma Spray: Study of the Coating Generation, *Ceram. Int.*, 1996, **22**(4), p 295-303
29. M. Pasandideh-Fard, V. Pershin, S. Chandra, and J. Mostaghimi, Splat Shapes in a Thermal Spray Coating Process: Simulations and Experiments, *J. Therm. Spray Technol.*, 2002, **11**(2), p 206-217
30. G.-J. Yang, X.-D. Xiang, L.-K. Xing, D.-J. Li, C.-J. Li, and C.-X. Li, Isothermal Oxidation Behavior of NiCoCrAlTaY Coating Deposited by High Velocity Air-Fuel Spraying, *J. Therm. Spray Technol.*, 2012, **21**(3-4), p 391-399